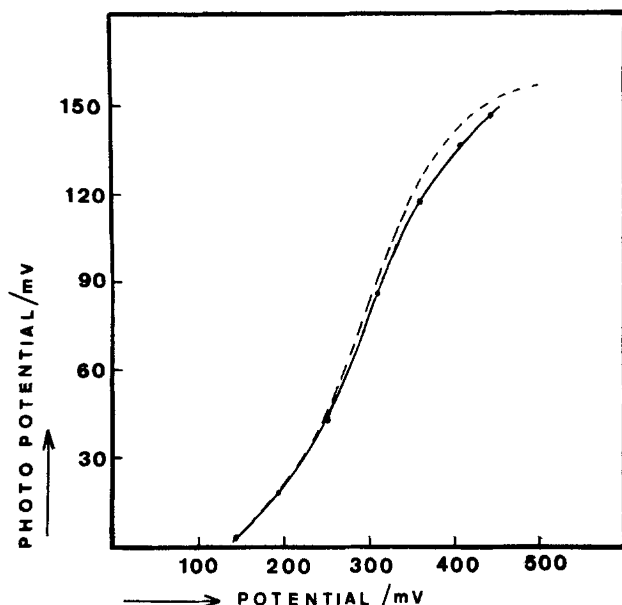

Fig. 7. The dependence of the photopotential for n-type Ge (sample as in Fig. 3) on dark surface potential V_S; $I_o = 10^{16}$ photons/cm^2-sec. Dashed line, calculated according to Johnson's method (4) assuming $pL_1 = 1.3 \times 10^{13}$ cm^{-3} (see text).

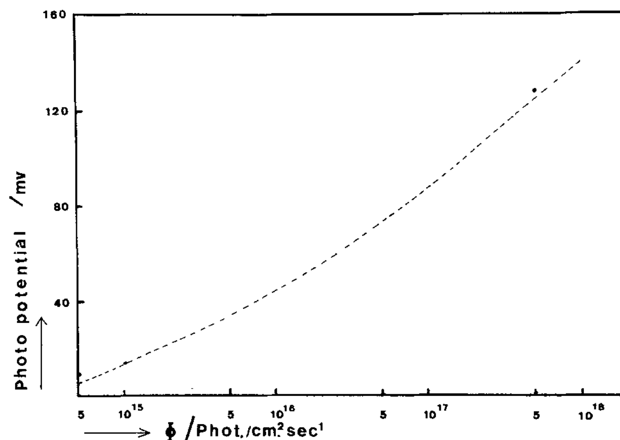

Fig. 8. Dependence of photopotential for n-type Ge (sample as in Fig. 2) on illumination intensity. V_S (dark) = 250 mV. Points are simulations and the dashed line was calculated by Johnson's method (4) assuming that the injection level was proportional to the light intensity and was 1.3×10^{13} cm^{-3} at an illumination intensity of 10^{16} photons/cm^2-sec.

Publication costs of this article were assisted by The University of Texas at Austin.

REFERENCES

1. D. Laser and A. J. Bard, *This Journal*, **123**, 1828 (1976).
2. M. D. Archer, *J. Appl. Electrochem.*, **5**, 17 (1975).
3. C. G. B. Garrett and W. H. Brattain, *Phys. Rev.*, **99**, 376 (1955).
4. E. O. Johnson, *ibid.*, **111**, 153 (1958).
5. S. W. Feldberg, in "Electroanalytical Chemistry," Vol. 3, A. J. Bard, Editor, chap. 4, Marcel Dekker, Inc., New York (1969).
6. H. Gerischer, *This Journal*, **113**, 1174 (1966).
7. V. A. Myamlin and Yu. V. Pleskov, "Electrochemistry of Semiconductors," pp. 30-50, Plenum Press, New York (1967).
8. A. Many, Y. Goldstein, and N. B. Grover, "Semiconductor Surfaces," chap. 4, John Wiley & Sons, Inc., New York (1965).
9. V. A. Myamlin and Yu. V. Pleskov, *op. cit.*, p. 18.
10. *Ibid.*, p. 55.
11. D. Laser and A. J. Bard, *This Journal*, **123**, 1837 (1976).
12. A. Rothwarp and K. W. Böer, "Progress in Solid State Chemistry," Vol. 10, p. 71, Pergamon Press, Oxford (1975).
13. V. A. Myamlin and Yu. V. Pleskov, *op. cit.*, p. 182.

Semiconductor Electrodes

IX. Digital Simulation of the Relaxation of Photogenerated Free Carriers and Photocurrents

Daniel Laser and Allen J. Bard*

Department of Chemistry, The University of Texas at Austin, Austin, Texas 78712

ABSTRACT

A digital simulation of the photoprocess at a semiconductor electrode is described. The simulation model accounts for photogeneration, recombination, and transport of excess free carriers within the semiconductor phase. The origin of the photopotential in the absence of faradaic current is elucidated. Quantitative current efficiency-potential curves for the photocurrents under a variety of conditions are calculated for n-type TiO_2 and these are compared to experimental results.

In previous papers in this series we have introduced the use of digital simulation methods for the treatment of semiconductor electrodes. In Ref. (1) the relaxation of free carriers following charge injection, with and without surface states, was described. In Ref. (2) a method of deriving the semiconductor electrode characteristics, equilibrium or steady state, at open circuit in the dark or under constant illumination, was presented. When a semiconductor electrode at equilibrium and in contact with solution is illuminated, a certain time elapses before the photoeffects are observed. During this time a redistribution of free carriers and charges in the electric field in the space charge region occurs. [When the semiconductor electrode/solution interface is blocked to charge transfer, the new distribution of free carriers in the space charge region under illumination will cause a change in the potential of the electrode (the photopotential effect).] Frequently, illumination of the electrode is accompanied by charge transfer to solution species and this gives rise to a photocurrent. For example, irradiation of n-type TiO_2 with light of energy larger than the bandgap energy will result in the oxidation of water (3, 4), while

* Electrochemical Society Active Member.
Key words: semiconductors, digital simulation, photoelectrochemistry, photogalvanic cells.

Downloaded 17 Feb 2009 to 146.6.143.190. Redistribution subject to ECS license or copyright; see http://www.ecsdl.org/terms_use.jsp

cathodic photocurrents arise at p-type semiconductor electrodes (5, 6). Numerous examples of photogalvanic effects and analytical treatments of these have been given (7, 8)

In this paper we treat the transient behavior of a semiconductor electrode following the onset of illumination and the photocurrents which are produced. The semiconductor electrode characteristics which affect the magnitude of the photocurrent are discussed and a comparison of the simulated light intensity-current and current-potential behavior with some experimental results given.

Relaxation of Photogenerated Carriers in the Absence of Faradaic Current: Physical Model

The rate of change of the concentration of excess free carriers (*e.g.*, holes, the minority carriers in an n-type semiconductor) during illumination is governed by their rate of generation by the adsorbed light, their recombination, and their transport

$$\partial \Delta p/\partial t = g(x) - (1/\tau_p)(n(x)/n_b)\Delta p + D_p(\partial^2 \Delta p/\partial x^2) + U_p \partial[\Delta(E \cdot p)]/\partial x \quad [1]$$

where $\Delta p = p(x) - p(x)^{eq}$, $\Delta E = E(x) - E(x)^{eq}$. A similar expression can be written for excess electrons, Δn. The electrical field vector in the x direction is governed by Gauss' law

$$\frac{d\Delta E(x)}{dt} = \frac{e}{\epsilon_0 \epsilon_r^\infty} \int^x \left[\frac{d}{dt}(p - n) \right] dx \quad [2]$$

Equations [1] and [2] were written in finite difference form by using the same space division and representation of fluxes given in Table I of Ref. (2); the actual expressions are given in the Appendix. The general notation and the terms in Eq. [1] and [2] are the same as those given in Ref. (1) and (2) and are discussed only briefly here. The generation function for free carriers by light, $g(x)$, can be written as

$$g(x) = I_0 a \exp(-ax) \quad [\text{cm}^{-3}\text{-sec}^{-1}] \quad [3]$$

I_0 is the incident light flux at the electrode surface ($\text{cm}^{-2}\text{-sec}^{-1}$) and a is the absorptivity of the light [cm^{-1}]. We assume here that all of the light absorbed leads to free carrier formation. The treatment is easily modified for less than unit efficiency of carrier formation by the introduction of a quantum efficiency factor. The term $(1/\tau_p)\Delta p$ is the usual expression (9) for the recombination rate of excess minority free carriers in the semiconductor bulk, where the process is assumed to be pseudo-first order with respect to the excess minority carriers (*i.e.*, $1/\tau_p = k_r n_b$, where n_b is the bulk concentration of electrons and k_r is the second order recombination rate constant). The term $n(x)/n_b$ is introduced to account for this effect inside the space charge region, where the concentration of electrons is not equal to the bulk value. The last two terms on the right-hand side of Eq. [1] are the divergence of the flux of excess free carriers by diffusion and migration. For a numerical calculation of the migration term, the properties of the semiconductor at equilibrium [$p(x)^{eq}$, $E(x)^{eq}$] have to be known. Similarly, calculation of the recombination term requires knowledge of $n(x)^{eq}$, in addition to $\Delta n(x)$. Thus, a simulation of the semiconductor electrode free carrier and electric field distribution in the dark at a given potential V_s, as given in Ref. (2), provides the initial conditions which precede simulation of the photoeffects. The usual simulation techniques were employed [see the Appendix and Ref. (10) and (11)]. Changes in Δp and Δn which occur during a short time interval, Δt, based on the carrier concentrations and fields from the previous time interval, were calculated. These changes are used to calculate new values of $p(x)$ and $n(x)$, as well as a new field distribution $E(x)$, by Eq. [2]. These new values are then used for calculation of the values of Δp and Δn in the next time interval, etc. The distribution of excess free carriers and electric field are mutually dependent, since $E(x)$ depends upon the charge and the migration of the free carriers depends upon the field.

Results

The distributions of excess carriers for an n-type TiO_2 electrode at two different times after the onset of illumination are shown in Fig. 1. In this example, the n-TiO_2 electrode at equilibrium in the dark was assumed to be initially biased positively ($V_s = 0.8$V) to form a depletion layer. In the time interval considered, only very slight changes in electric field are observed. The changes in the charge density distribution, although noticeable, are still very small compared to the charge density at equilibrium or to the changes in charge density which exist at the steady state. Consider some aspects of the relaxation process which can be observed from the transient behavior. The generation function is an exponential one with respect to distance from the surface so that with the semilog axes of Fig. 1 it would be drawn as a straight line with a slope of $-a$. However, except for the very first instants following the onset of illumination, the shape of the perturbation (the light generation function) is not apparent. Because of the rapidity of the transport processes in the semiconductor phase, the distribution of excess free carriers reflects rather the momentary existing driving forces (electric fields and concentration gradients). Thus, the excess holes accumulate at the semiconductor surface (assuming no outlet to solution), while the electrons accumulate near the space charge region/bulk boundary. At this stage, some of the holes which are produced outside the space charge region and which escape recombination enter the space charge region by diffusion. Only at a later time, when the surface concentration of holes increases further, are they reflected back from the surface by diffusion, so that at the steady state [as in Ref. (2)] a flux of holes leaves the space charge region toward the bulk. At this time the concentration excess of holes outside the space charge region is about equal to the concentration excess of electrons ($\Delta n = \Delta p$). This steady-state situation could not be achieved within the time domain of the transient simulation. The reason for this will be discussed in some detail, because it is directly related to the general problem of simulation of the photoprocess. The steep concentration and field profiles which exist inside the space charge region require a

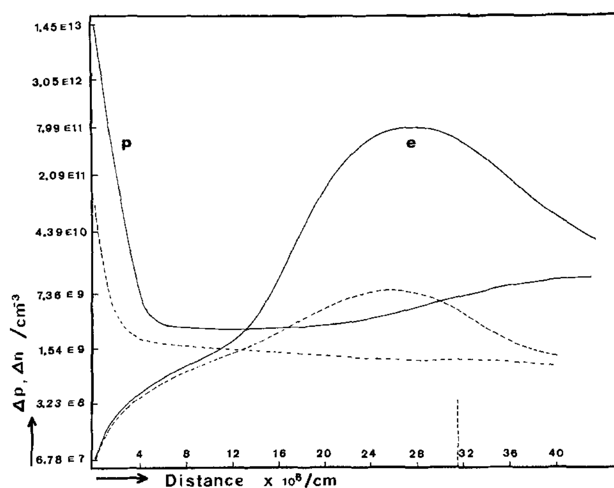

Fig. 1. Excess carrier concentrations in n-type TiO_2 (dashed line) 1.44×10^{-11} sec and (solid line) 1.16×10^{-9} sec after turning on illumination (10^{16} photons cm^{-2} sec^{-1}). $V_s = 0.8$V (in dark); $n^\circ = 10^{17}$ cm^{-3}; $p^\circ = 0$; $\epsilon_r = 100$ esu; $U_n = 100$ and $U_p = 50$ $\text{cm}^2\text{-sec}^{-4} \cdot \text{V}^{-1}$; $a = 5 \times 10^4$ cm^{-1}; $\tau_p = 10^{-9}$ sec. Vertical dashed line shows space charge region/bulk semiconductor boundary.

Downloaded 17 Feb 2009 to 146.6.143.190. Redistribution subject to ECS license or copyright; see http://www.ecsdl.org/terms_use.jsp

fine division of space elements ($\Delta x \simeq$ 20-50Å) to represent the quantities there to a sufficient accuracy in the digital simulation. Because of this, combined with the high value of the transport coefficients of the free carriers, a very short time interval must be used as a simulation time step (*ca.* 10^{-14} sec) and the total simulated time is limited to the nanosecond range even after 10^5 simulation steps. For reasonable fluxes of light to be calculated (*e.g.*, 10^{16} photons cm^{-2} sec^{-1}), the excess of free carriers added to the space charge region within this time interval is far smaller than the amount which will be present there at the steady state to produce the photopotential. An attempt to overcome this problem by using higher light fluxes or slower transport coefficients (which, numerically, have the same effect) results in a distorted picture in which the generation of carriers is very exaggerated with respect to their transport. Thus the transport processes (migration and diffusion) dominate all others. The speed at which these driving forces, especially inside the space charge region, dissipate a large portion of any local perturbation (provided it is not too large) is what underlies the possibility of using the Boltzmann distribution in cases where actual equilibrium does not exist (7, 8). The simulated transient behavior allows us to deduce the sequence of events which leads to the steady state and causes the photopotential effect. This is shown schematically in Fig. 2. The charge density distributions at equilibrium in the dark and under illumination are given in Fig. 2a. Figure 2b shows the redistribution of the charge density caused by the changes Δp and Δn in the light. The total charge is conserved and so is the surface field, but its distribution shows an accumulation of positive charge at the surface and a loss of positive charge at the space charge region/bulk boundary (where the excess of electrons which accumulate there compensates for the diffuse positive charge of the space charge region). The corresponding electric field distributions are shown in Fig. 2c. The area between the field curves, *i.e.*, the integration of the difference in the electric field with respect to distance from the bulk semiconductor to the surface, is the decrease in surface potential due to illumination, the photopotential

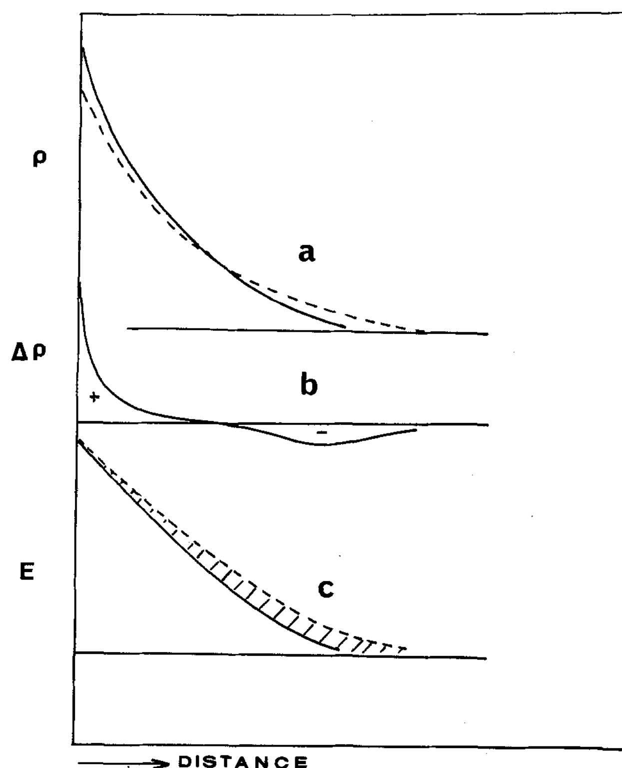

Fig. 2. Schematic representation of the production of the photopotential. (a) Charge density (ρ) distribution in the space charge region (dashed line) in the dark; (solid line) under illumination. (b) Excess charge density distribution with illumination due to redistribution of excess carriers as shown in Fig. 1, ($\Delta\rho^+ = \Delta\rho^-$). (c) Electrical field (dashed line) in the dark and (solid line) under illumination. The area between the curves represents the photopotential.

Photocurrent in the Absence of Kinetic Complications

If charge transfer across the semiconductor/solution boundary is possible, the situation differs from the open-circuit case described above. Two extreme cases can be considered. If the rate constant for charge transfer is infinitesimal, the open-circuit case, which is characterized by very small faradaic currents and the photopotential effect, is approached. At the other extreme, if the charge transfer to solution is limited only by the combined effect of generation/recombination and transport of carriers within the semiconductor phase, only a small accumulation of excess free carriers occurs leading to a smaller photopotential and larger faradaic currents. Thus, the rate constant for charge transfer to solution will have a key role in determining both the photocurrent and the electrical state of the semiconductor.

We simulate here the fast charge transfer case and calculate the photocurrent which is determined by the processes within the semiconductor phase. We use n-type TiO_2, a stable semiconductor electrode for which the photocurrent has been widely described (3, 4), as a model. The very low concentration of minority carriers (holes) in this sample somewhat simplifies the calculation because no oxidation current (hole injection to solution) exists in the dark.

The photocurrent density due to photogenerated holes within the semiconductor biased to positive potentials is expressed as the product of the charge transfer rate constant k_p ($cm \cdot sec^{-1}$) and the hole concentration at the surface ($x = 0$) (or in the simulation for space element, $K = 1$)

$$i_{p,f} = ek_p p(o) \quad [4]$$

The rate constants were chosen to be sufficiently large that the steady photocurrent calculated in the simulated time domain was independent of the value of k_p. The surface concentration of holes was found to be inversely proportional to k_p. The effect of the magnitude of k_p is shown in Fig. 3. The electron distribution is also affected by k_p, because for every hole which is injected into the solution, an electron is collected by the metallic contact to the semiconductor electrode

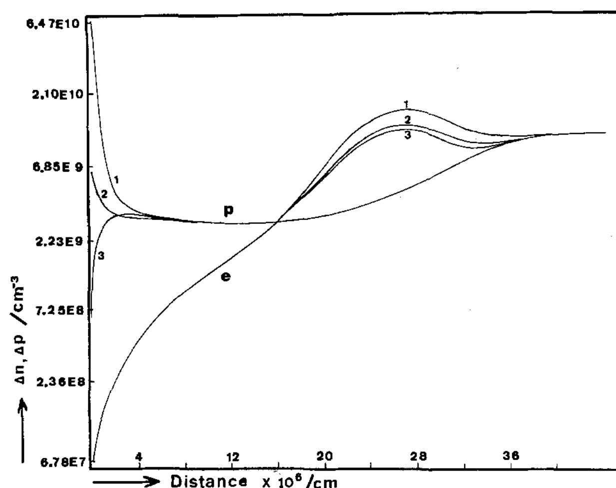

Fig. 3. Effect of k_p on the concentration profiles of excess free carriers. All conditions as in Fig. 1, except with holes transfer to solution with k_p values of (1) 1.39×10^5; (2) 1.39×10^6; (3) $k_p = 1.38 \times 10^7$ cm/sec. In all cases the calculated photocurrent, $i_{p,f}$, was 1.437 mA.

Downloaded 17 Feb 2009 to 146.6.143.190. Redistribution subject to ECS license or copyright; see http://www.ecsdl.org/terms_use.jsp

and is delivered to the counterelectrode. Although the effect of k_p is most prominent at the semiconductor surface, it also determines the whole level of excess holes inside the space charge region and hence the flux of holes which will enter this region. Under actual conditions the situation may be far more complex because k_p may depend upon the potential drop in the Helmholtz layer at the semiconductor/solution interface, $\Delta\phi_H$, *e.g.*, it could be given by $k_p^o \exp(\beta e \Delta\phi_H/kT)$ and where k_p^o may have a much smaller value than that used in the simulation. At the instant after illumination only a small photocurrent is expected, resulting in a pronounced accumulation of excess carriers in the space charge region, in a manner similar to that for the open-circuit case. This accumulation causes a photopotential to be built up gradually, which in a potentiostatic experiment will result in a gradual change in $\Delta\phi_H$ and in an increase in k_p. At the steady state the charge transfer rate will be sufficiently fast to prevent any further accumulation of excess free carriers inside the space charge region. We did not simulate this suggested sequence of events which extends over two completely different time domains. Moreover, k_p could not be made too small because under these conditions, even after a lengthy computation, a steady state was not achieved. Therefore, we can only speculate that as long as migration is the predominant driving force (high fields and band bending) and k_p is not so small that a high accumulation of excess carriers is produced inside the space charge region thus changing considerably the fields there, only a minor dependence of photocurrent on k_p is expected. At low band bending, on the other hand (which would usually occur at the foot of the photocurrent-potential wave), diffusion may be the main transport process. The photocurrent will then strongly depend upon the diffusional flux of the holes inside the space charge region and towards the surface, which in turn will be determined by the concentration profile present and thus on k_p.

Results

Photocurrent-potential curves assuming rapid charge transfer to solution under several different sets of conditions were simulated (Fig. 4). Curve a represents the steady-state currents for the electrode initially (in the dark) held at the indicated potential where all of the imposed potential is assumed to drop inside the semiconductor space charge region. No photopotential is observed. The dashed line a shows the calculated curve if electrons are allowed to cross the surface as well, to reduce the species just formed by the hole injection process, or to react with holes at the surface at a rate which is proportional to the absolute concentration of electrons at the surface. Both processes will have the same effect in reducing the net oxidation current. This back-reaction effect could be of importance, since the photosensitized oxidation at the semiconductor electrode frequently produces a species which is thermodynamically reducible at the electrode potential. For any value for the rate constant, k_n, chosen for this "back-reaction" effect, the observed photocurrent is found to rise very steeply (almost discontinuously) with potential. This steep rise is caused by the fact that the absolute electron concentration at the surface is an exponential function of potential. Such abrupt rises in photocurrent are not observed experimentally. A calculation in which the excess of electrons at the surface, rather than their absolute numbers, determines their contribution to the photocurrent is shown as curve a″. A simple model for surface recombination, similar to that which was presented previously (1) results in the expression

$$i_f = e[k_p \Delta p(o) - k_n \Delta n(o)] \quad [5]$$

For the case under consideration, for holes, $\Delta p \simeq p$, while for electrons, $\Delta n = n - n^{eq}$. This effect modifies somewhat the foot of the photocurrent-potential wave.

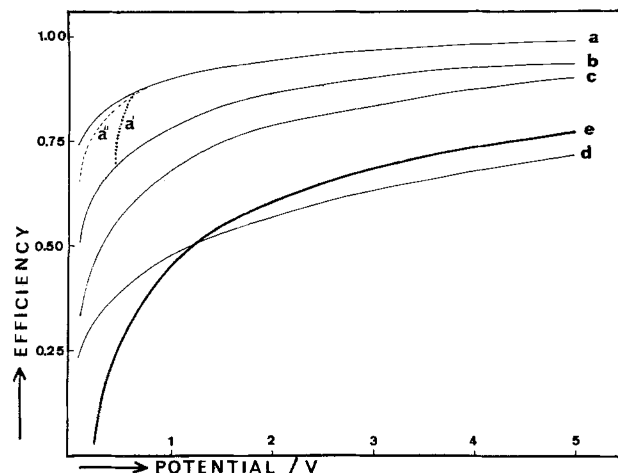

Fig. 4. Simulated photocurrent-potential curves for n-TiO_2. Electrode as in Fig. 1, $I_o = 10^{16}$ photons $cm^{-2}sec^{-1}$, $k_p = 2.78 \times 10^6$ cm/sec, except as noted below. Efficiency $= i_{p,f}/I_o$, with $i_{p,f}$ given in holes per second. (a) $\tau_p = 10^{-9}$ sec; (a′) as in (a), assuming electrons cross to solution at a rate proportional to their absolute number at the surface, with a rate constant $k_n = 1.39 \times 10^6$ cm-sec^{-1}; (a″) as in (a) assuming electrons cross to solution at a rate proportional to their excess number at the surface, $k_n = 1.39 \times 10^6$ cm-sec^{-1}; (b) as in (a″), $a = 3 \times 10^4$ cm^{-1}; (c) as in (b), $\tau_p = 10^{-10}$ sec; (d) $a = 3 \times 10^4$ cm^{-1}, $\tau_p = 5 \times 10^{-11}$ sec, $n^\circ = 4 \times 10^{17}$ cm^{-3}; (e) experimental efficiency curve for a single crystal TiO_2 for water photo-oxidation (c axis normal to solution) measured at 375 nm; solution pH = 4.0; the potential axis in this case is the electrode potential *vs.* SCE.

At more positive potentials the excess of surface electrons is negligible (since they are repelled from the surface) compared to the excess of holes, and no "back-reaction" effect is noticed.

Two other factors govern the photocurrent and enter into the simulation. The first is the bulk recombination rate constant for the excess minority carriers ($1/\tau_p$). This influences the number of holes which are generated outside the space charge region which will be collected by the space charge region and delivered to the surface. Photogenerated holes which are produced at a distance greater than $\sqrt{\tau_p D_p}$ from the space charge region/bulk boundary are practically lost and will not contribute to the photocurrent. The effect is illustrated by Fig. 5. An extremely high bulk recombination rate constant can even reverse the direction of

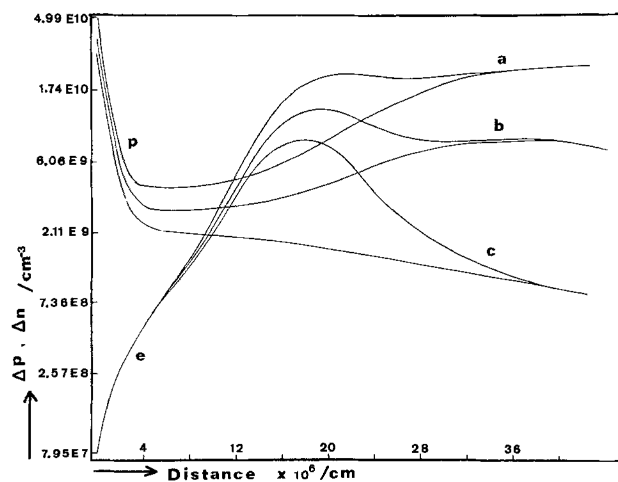

Fig. 5. Effect of bulk recombination rate constant for excess holes on the photocurrent and concentration profiles of excess free carriers. Electrode and illumination as in Fig. 1; $V_s = 0.4$V. (a) $\tau_p = 10^{-9}$ sec, $i_{p,f} = 1.096$ mA; (b) $\tau_p = 10^{-10}$ sec, $i_{p,f} = 0.8881$ mA; (c) $\tau_p = 10^{-11}$ sec, $i_{p,f} = 0.7186$ mA.

Downloaded 17 Feb 2009 to 146.6.143.190. Redistribution subject to ECS license or copyright; see http://www.ecsdl.org/terms_use.jsp

diffusion of holes, resulting in a hole flow from the space charge region to the bulk semiconductor. A second factor, directly related to the first, is the relative dimension of the space charge region to the light penetration depth. A more efficient photoprocess will be observed if practically all of the photogeneration process of free carriers occurs within the space charge region where the excess of holes suffer very little recombination and are delivered promptly to the surface by migration. The depletion layer thickness is determined by the potential imposed on the semiconductor electrode and its width can be taken as being proportional to the square root of the imposed potential (12). The upper quantum efficiency limit, which asymptotically approaches unity, represents the situation of a high surface potential resulting in an extended space charge region in which all of the light is absorbed. All of these simulated observations are consistent with Gartner's approximate treatment of the subject (12). Curves b, c, and d in Fig. 4 show the calculated results for variations in a, τ_p, and N_D (which influences the thickness of the space charge region). Curve e shows an experimental efficiency curve measured at a single crystal of TiO_2 in a pH = 4.0 solution with a monochromatic light of wavelength 375 nm. While the calculated saturation current can be adjusted to fit the experimental one, a larger discrepancy is revealed between the simulated and the experimental curve on the rising portion of the wave. A better fit to the experimental results will probably require consideration of the previously discussed kinetics of the charge transfer and other solution processes as well.

Acknowledgment

The support of this research by the National Science Foundation (MPS74-23210) is gratefully acknowledged.

Manuscript submitted Feb. 3, 1976; revised manuscript received Feb. 7, 1976.

Any discussion of this paper will appear in a Discussion Section to be published in the June 1977 JOURNAL. All discussions for the June 1977 Discussion Section should be submitted by Feb. 1, 1977.

Publication costs of this article were assisted by The University of Texas at Austin.

APPENDIX

Equation [1], the corresponding equation for electrons, and Eq. [2] were simulated according to the procedure shown in the Appendix of Ref. (1) and the space division and digital notation which were used in Table I of Ref. (2). For holes in the case of n-TiO_2, with a bandgap of 3.0 eV, we can write

$$p^{eq}\Delta E \simeq 0 \quad \text{and} \quad \Delta p \Delta E \simeq 0 \qquad [A\text{-}1]$$

$p^o = p^{eq} \simeq 0$ across the whole semiconductor. The change of concentration of holes in element K within a time interval Δt is

$$\Delta p_K = L_K - (\Delta t/\tau_p)\cdot(n_K/n_b)\cdot p_K + DMP(p_{K-1} - 2p_K + p_{K+1}) + 0.5\, UMP\{E_{K+1}(p_K + p_{K+1}) - E_K(p_K + p_{K+1})\} \qquad [A\text{-}2]$$

For electrons, a more complicated expression arises because of the importance of the term $U_n\partial\Delta(E\cdot n)/\partial x$

$$\Delta(E\cdot n) = E^{eq}\Delta n + n^{eq}\Delta E \qquad [A\text{-}3]$$

where $\Delta n = n - n^{eq}$ and $\Delta E = E - E^{eq}$. Here, the term $n^{eq}\Delta E$ cannot be neglected, especially near the space charge region boundary. The resulting expression for electrons is

$$\Delta(\Delta n) = L_K - (\Delta t/\tau_p)(n_K/n_b)p_K + DMN(\Delta n_{K-1} - 2\Delta n_K + \Delta n_{K+1}) + 0.5\, UMN\{E_K{}^{eq}(\Delta n_K + \Delta n_{K-1}) - \Delta E_{K+1}{}^{eq}(\Delta n_K + \Delta n_{K+1}) + \Delta E_K(n_K{}^{eq} + n_{K-1}{}^{eq}) - \Delta E_{K+1}(n_K{}^{eq} + n_{K+1}{}^{eq})\} \qquad [A\text{-}4]$$

In Eq. [A-2] and [A-4] the following terms apply

$$L_K = (I_o a)\exp[-a(K - \tfrac{1}{2})\Delta x] \qquad [A\text{-}5]$$

$$DMN = D_n\Delta t/\Delta x^2 \qquad DMP = D_p\Delta t/\Delta x^2$$

$$UMN = U_n\Delta t/\Delta x \qquad UMP = U_p\Delta t/\Delta x$$

The resulting change in the electric field caused by changes in Δp_K and Δn_K is

$$\Delta E_K = (e\Delta x/\epsilon_o\epsilon_r)(\Delta p_K - \Delta n_K) + \Delta E_{K+1} \qquad [A\text{-}6]$$

The following boundary conditions apply

$$\Delta p_{K\to\infty} = 0,\quad \Delta n_{K\to\infty} = 0,\quad E_{K\to\infty} = 0 \qquad [A\text{-}7]$$

The calculation cannot be extended in reasonable simulation times to K values that rigorously will satisfy the conditions of Eq. [A-7]. Instead, the following boundary condition was chosen

$$\Delta p_{KMAX} = \Delta p_{KMAX-1}\exp\{-\Delta x/(\tau_p D_p)^{1/2}\} \qquad [A\text{-}8]$$

$$\Delta n_{KMAX} = \Delta p_{KMAX} \quad \Delta E_{KMAX} = 0$$

where $\Delta x \cdot KMAX$ is far outside the space charge region but still not in the bulk.

For the first element ($K = 1$) (the semiconductor surface) within the semiconductor, only transport to the second element occurs. Charge transfer to solution is expressed, when desired, as the product of a rate constant k_p with the hole concentration in the first element. The initial conditions are the equilibrium distribution of carriers and electrical fields which are first obtained by the simulation procedure previously described (2).

LIST OF SYMBOLS

a	absorptivity of light
D_p, D_n	diffusion coefficients of holes, electrons
$E(x)$	electric field
$E(x)^{eq}$	electric field at equilibrium
$\Delta E(x)$	change in electric field with respect to equilibrium $[E(x) - E(x)^{eq}]$
$g(x)$	generation function of light
i_f	total faradaic current
$i_{p,f}$	faradaic current due to holes
I_o	flux of light
k_p, k_n	charge transfer rate constants for holes, electrons
k_r	recombination rate constant
K	simulation distance index
$n(x)$	electron concentration
$n(x)^{eq}$	electron concentration at equilibrium
n_b	electron concentration in bulk semiconductor
Δn	excess concentration of electrons $[n(x) - n(x)^{eq}]$
$p(x)$	hole concentration
$p(x)^{eq}$	hole concentration at equilibrium
p_b	hole concentration in bulk semiconductor
Δp	excess concentration of holes $[p(x) - p(x)^{eq}]$
Δt	simulation time interval
U_p, U_n	mobility of hole, electron
x	distance from electrode surface
Δx	simulation space element thickness
β	transfer coefficient
$\Delta\phi_H$	potential drop in the Helmholtz layer
ϵ_o	permittivity of free space (mks)
ϵ_r	dielectric constant
τ_p	average lifetime of excess minority carrier (hole) in bulk n-type semiconductor

REFERENCES

1. D. Laser and A. J. Bard, *This Journal*, **123**, 1828 (1976)
2. D. Laser and A. J. Bard, *ibid.*, **123**, 1833 (1976).
3. P. J. Boddy, *ibid.*, **115**, 199 (1968).

Downloaded 17 Feb 2009 to 146.6.143.190. Redistribution subject to ECS license or copyright; see http://www.ecsdl.org/terms_use.jsp

4. A. Fujishima and K. Honda, *Nature*, **238**, 37 (1972).
5. D. Laser and A. J. Bard, *J. Phys. Chem.*, **80**, 459 (1976).
6. H. Gerischer and I. Mattes, *Z. Phys. Chem. (Frankfurt)*, **49**, 112 (1966).
7. H. Gerischer, *This Journal*, **113**, 1174 (1966).
8. C. G. B. Garrett and W. H. Brattain, *Phys. Rev.*, **99**, 376 (1955).
9. A. Many, Y. Goldstein, and N. B. Grover, "Semiconductor Surfaces," chap. 2, John Wiley & Sons, Inc., New York (1965).
10. S. W. Feldberg, in "Electroanalytical Chemistry," Vol. 3, A. J. Bard, Editor, chap. 4, Marcel Dekker, Inc., New York (1969).
11. S. W. Feldberg, *J. Phys. Chem.*, **74**, 87 (1970).
12. W. W. Gärtner, *Phys. Rev.*, **116**, 84 (1959).

Analysis of Multiple Reaction Sequences in Flow-Through Porous Electrodes

Richard Alkire* and Ronald Gould**

Department of Chemical Engineering, University of Illinois, Urbana, Illinois 61801

ABSTRACT

The role of multiple reactions in flow-through porous electrodes has been investigated theoretically. The reaction sequences studied include simultaneous deposition of several metals, deposition of a metal in the presence of a redox system, and an ECE sequence which is characteristic of many electro-organic synthesis reactions. The model accounts for mass transport, multiple charge transfer reactions, homogeneous chemical reactions, ohmic and geometric parameters. Results are compiled in a series of graphs which elucidate electrode behavior over a wide region of parameter space.

One advantage of electrochemical processes is that a high level of selectivity for a desired reaction product can often be achieved through careful control of the potential under which reaction proceeds. On the other hand, the attainment of economically high volumetric reaction rates often requires optimizing around competing needs for large surface area, adequate mass transfer, and low ohmic resistance. Although flow-through porous electrodes are advantageous for achieving high reaction rates per unit volume, these devices often exhibit substantial potential variations over their interior surface so that the original electrochemical advantage of selectivity may thereby be lost. The purpose of this investigation is to develop theoretical methods for predicting the selectivity of flow-through porous electrodes in systems where multiple reactions occur, and to illustrate how such predictions can be compiled for use in engineering design.

Literature Review

The use of fixed bed porous electrodes with a single electrode reaction has been recently reported for stripping copper (1), depositing antimony (2) and copper (3-5), carrying out redox reactions with iron (6) and ferricyanide couples (5, 7, 8), detecting dissolved gases (9-11), and for precipitating anionic species (12). Earlier work has been reviewed with emphasis on battery applications (13) for which a single electrode reaction is the preferred mode of operation. The extensive publications of Sioda, reviewed in Ref. (13), are especially noteworthy since they established many experimental procedures and theoretical methods of analysis. Many additional porous electrode studies are known which involve multiple electrochemical reactions in order to accomplish simultaneous removal of several metal ions from mixed solutions (14-21); separation of quinones (22), radioactive nuclides (23), and halide ions (24); and reduction of metal ions in the presence of competing reactions (25). Reaction schemes involving coupled electrochemical and homogeneous chemical steps have also been used in porous electrode cells for coulometric and preparative applications (12, 26-29), and for electro-organic synthesis applications (30-36). It is abundantly clear that multiple reaction sequences are commonly encountered in many fixed bed porous electrode applications.

Theoretical considerations of multiple reaction effects in porous electrodes have led to the development of simple criteria for choosing the flow velocity and applied current such that (*i*) the potential distribution is sufficiently uniform that side reactions are avoided (8, 13, 37), or (*ii*) the residence time is convenient for maximizing the production of an intermediate species in a sequential reaction (27). In both cases, the approximate procedures are based on the need to attain a high degree of selectivity in the presence of multiple reactions. Therefore it seems appropriate to develop a more extensive theoretical basis for predicting the current and potential distribution behavior of porous electrodes in the presence of multiple homogeneous and heterogeneous reactions.

* Electrochemical Society Active Member.
** Electrochemical Society Student Member.
Key words: porous electrode, mathematical model, multiple-metal deposition, metal-redox reactions, current distribution.

Theoretical Formulation

The geometry of the porous electrode system under study is indicated in Fig. 1a. Electrolyte flows in the direction of the y coordinate; the electrode is of thickness l. The counterelectrode may be located either upstream or downstream from the porous electrode; in Fig. 1a, a downstream location is shown. Other details of cell construction are not shown since they are not included in the model equations. Electrolyte flows through the porous electrode, supplying reactants to the interior surface where electrochemical reaction occurs. The local reaction rate is a function of position since the potential and species concentrations vary along the reactor length owing to ohmic and transport limitations.

Figure 1b illustrates how the processes in the interior region of the porous electrode are envisioned by the model. The solid surface of the interior region, upon which electrochemical charge transfer occurs, is of arbitrary shape and is accounted for in the model only by a specific area term. The species concentration distributions at the solid surface, $c_i^s(y)$, are different from the species concentration distributions in the well-mixed core, $c_i(y)$, owing to the presence of a mass transfer diffusion layer between core and surface. The diffusion layer is assumed to occupy only a small fraction of the electrolyte volume so that (*i*) if homo-

Downloaded 17 Feb 2009 to 146.6.143.190. Redistribution subject to ECS license or copyright; see http://www.ecsdl.org/terms_use.jsp